INSTITUTE OF PHYSICS PUBLISHING SEMICONDUCTOR SCIENCE AND TECHNOLOGY

Semicond. Sci. Technol. **21** (2006) 860–865 doi:10.1088/0268-1242/21/7/006

# Arrays of periodic submicron conductive links in Si covered by $SiO_2$ formed by polarized laser irradiation

**Yougui Liao and Michel Meunier**

Laser Processing Laboratory, Department of Engineering Physics, Ecole Polytechnique de Montreal, Case Postale 6079, Succursale. Centre-ville, Montréal, Québec, H3C 3A7, Canada

E-mail: liao.yougui@polymtl.ca and michel.meunier@polymtl.ca

Received 7 November 2005, in final form 2 March 2006
Published 23 May 2006
Online at stacks.iop.org/SST/21/860

**Abstract**

Arrays of periodic submicron conductive links were fabricated in silicon covered by $SiO_2$ when polarized frequency doubled Nd:YAG pulsed laser irradiation is focused on the gap between two highly doped regions. The principle of the process is based on the fact that the laser forms periodic melting in silicon, thus inducing preferential dopant diffusion and creating an array of fine conductive links between the highly doped regions. A scanning capacitance microscopy (SCM) was employed to detect these submicron structures and to measure their electrical properties. It was found that between two and seven submicron conductive links are observed in a focused spot size of 3 $\mu$m and their number depends only on the laser intensity ranging from 3.10 W to 3.75 W, while their average width (151–300 nm) and depth (108–147 nm) strongly depends on both the laser intensity and number of laser pulses. The resistances of these links are between 363–493 Ω and the effective average doping levels are from $1.5 \times 10^{18}$ to $2.4 \times 10^{19}$ $cm^{-3}$.

## 1. Introduction

For many years, ripples [1–5] formed under intense laser irradiation on silicon materials have been considered to be formed at a temperature close [1] to the melting threshold. This spontaneous periodic surface structures formed after irradiation of a single or multiple uniform laser beam(s) [6] operating at optical wavelengths from the infrared to the ultraviolet region, with pulse durations ranging from continuous wave (cw) to femtosecond pulses [5–8] were frequently observed on the surface of a variety of blank materials such as dielectrics, semiconductors and metals. The spatial orientation and distribution of the crests and valleys of the ripples are always found to be related to the wavelength ($\lambda$) [9] and the incident electric field [10], such as polarization and the angle of the laser radiation. Emmony *et al* [3] for the first time proposed that a scattering centre on the surface might be responsible for the observed periodic topography. It has been suggested that theses ripples arise from standing waves produced by instability and developed as a result of interference of incident laser light with scattered electromagnetic waves from a surface disturbance [2, 11, 12]. When the light intensity is sufficiently high, the melting threshold of the surface is periodically exceeded, and thus rapid regrowth of a thin layer of molten material induces a constructive topography. The ripple periods are mostly found to follow Rayleigh's diffraction criterion [10, 12].

As recently noted by our research group [14], periodic coexisting of liquid and solid can be formed in Si material covered by $SiO_2$ during a polarized laser irradiation with a specific laser power range and highly controlled sample surface conditions. Following the suggestion of Guosheng *et al* [10] and by considering that the laser beam of wavelength $\lambda$ is normal to the sample surface, the periodic spacing should be scaled and becomes to about $\Lambda = \lambda/n$, where $n$ is the index of refraction of the surrounding media. For instance, a periodicity of about 360 nm was recently observed by TEM (transmission electron microscopy) on these $SiO_2$/Si systems due to oxygen diffusion into liquid silicon [14] (where $n_{SiO_2} = 1.5$), when the sample was irradiated by a focused (diameter of ~3 $\mu$m) Nd:YAG frequency doubled laser ($\lambda = 532$ nm).

  

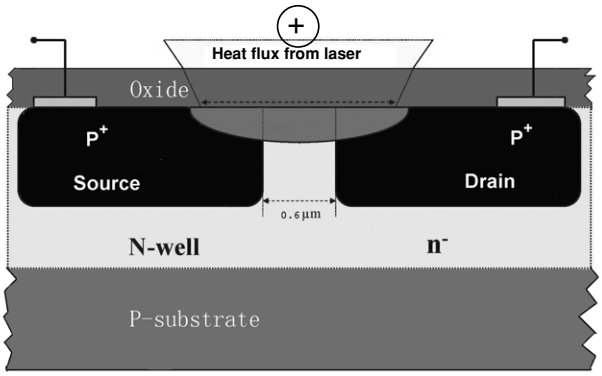


**Figure 1.** Schematic showing the principle of laser fine tuning technology with a gateless MOSFET structure. Upon silicon melting induced by laser irradiation, dopants diffuse from the source and drain, thus creating a conductive link. The polarization orientation is also shown.

Recently, laser fine tuning (LFT) technology [13] has been developed to fabricate highly accurate resistors in silicon with a visible focused pulsed laser beam irradiating the gap between two heavily doped regions of a gateless MOSFET structure covered by $SiO_2$. When the laser power is as large as normally used during the LFT fabrication, the dopants, such as boron atoms [15], in the heavily doped nominal source and drain, diffuse into the uniformly melted regions of the gap caused by laser irradiation and thus, form a 'large' conductive link with certain resistance value depending on the temporal and spatial temperature distribution and initial dopant distribution in the source and drain regions. Note that we have already shown [13, 14] that the dopants are essentially diffusing only in the liquid state as its diffusion length in the solid is estimated to be less than a few nanometres. In this paper, we use laser induced periodic melting in silicon covered by $SiO_2$ to form an array of submicron conductive links by focusing the laser in the gap between the heavily doped regions, as shown in figure 1. Now, in a particular laser power range, we will show that periodic melting will lead to a periodic dopant distribution and the formation of an array of submicron conductive links joining the two heavily doped regions. These structures were detected and analysed by a SCM (scanning capacitance microscopy) technique, which has been developed as a reliable analysis tool for two-dimensional (2D) dopant evaluation during the scaling of microelectronic devices [16]. The electrical behaviours related to dopant and oxygen distribution is also characterized by analysing the $dC/dV \sim V$ dependence.

## 2. Experimental details

The polarized laser induced periodic melting processes were carried out with a frequency doubled Nd:YAG laser ($\lambda = 532$ nm) at a pulse width of 80 ns irradiating the samples during 100 $\mu$s with 30 to 100 pulses. The incident laser power, focused on the surface of the chips, was maintained at either 3.75 W or 3.10 W and its polarization is oriented perpendicularly to the $p^+$–n–$p^+$ structure, as shown in figure 1. According to light reflection measurements during laser irradiation on our samples, only about 29% of the incident laser intensity was absorbed by the thin Si layer close to the interface between the dielectrics and the Si substrate. Therefore, the intensities absorbed by Si materials were about 1.08 W and 0.9 W, respectively, for the two laser energies above.

The initial gateless MOSFET devices were fabricated by a conventional CMOS process including ion implantation and thermal annealing steps. Although we do not know the fabrication parameters, it was verified that those initial devices consisted of two heavily doped p-type regions (boron concentration at $\sim 5 \times 10^{19}$ atoms $cm^{-3}$) having a doped depth of 170 nm and separated by a lightly As doped gap (concentration at $\sim 10^{15}$ atoms $cm^{-3}$) with a distance of 600 nm. In order to remove the very thick dielectric multilayers with a thickness of $\sim 8$ $\mu$m, including $SiO_xN_y$, $Si_3N_4$ and $SiO_2$, covering the interesting laser irradiated area, the samples were first of all dipped into 49% HF solution for 10 min under a standard clean room condition at a temperature of 21 °C. This aggressive chemical solution was used to rapidly remove most dielectrics including $Si_3N_4$ materials. Based on a cross-sectional TEM observation of these etched devices, it was verified that the bottom $SiO_2$ ($\sim$500 nm) was not removed. To complete the removal of the remaining dielectrics, the samples were cleaned with deionized (DI) water and, then, dipped immediately into 1% HF solution for 6 min. Before SCM measurements, the samples remain in a clean air condition for more than 10 days in order to grow a thin native oxide layer of $\sim$1–2 nm [17] covering the samples' surface. It should be pointed out that the thin oxide layer is important as it forms a MOS structure and enhances the SCM signals [18].

Measurements were carried out, in ambient conditions, by a SCM system (Digital Instruments, Dimension 3100 Model) using a standard AFM (scanning atomic force microscope) with a metallized probe. The metallic probe tip, scanning on semiconductor samples in contact mode, forms a MOS structure together with the thin oxide layer, as shown in figure 2. The dc bias voltage ($V_{dc}$) is applied to the sample and the tip is grounded. All SCM measurements were performed with a 90 kHz ac modulation voltage. In $dC/dV \sim V$ measurements, the $V_{dc}$ was swept between $-12$ V and +12 V when the probe was fixed at one position. When a negative dc offset is applied to the sample, there are three capacitors as shown in figure 2($a$), including a capacitance ($C_0$) formed with the oxide layer, a capacitance ($C_{d1}$) formed due to depletion at the Si near surface, and a capacitance ($C_{sub}$) formed due to the depletion in the p–n junction between the n-well and p-substrate. The SCM imaging principle is based on the fact that the tip-sample capacitance decreases due to the depletion layer generated in the SCM structure [19]. When a negative $V_{dc}$ is applied, the overall capacitance ($C_T$) is formed by three capacitances in series and then the overall $\Delta C_T$ can be calculated as

$$\frac{\Delta C_T}{C_T^2} = \frac{\Delta C_{d1}}{C_{d1}^2} + \frac{\Delta C_{sub}}{C_{sub}^2} + \frac{\Delta C_0}{C_0^2}. \quad (1)$$

Since $C_0$ is relatively small and constant, it does not contribute to the measurements. Now since the capacitance area $A_C$ for $C_{sub}$ of 100 $\mu m^2$ is approximately $10^6$ times larger than the one for $C_{d1}$ and since the effective dopant concentration $N_B$ given by $N_B^{-1} = N_A^{-1} + N_D^{-1}$ is $N_{B,sub} \approx 10^4 N_{B,d1}$, one can estimate that $C_{d1} \approx 10^{-4} C_{sub}$ for typical dc and ac applied voltages by using $C \propto A_C \sqrt{N_B}$ for an abrupt p–n junction

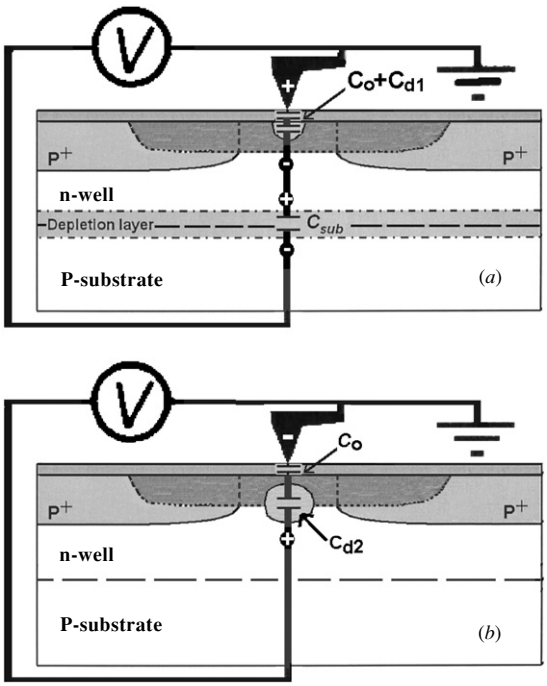


**Figure 2.** Schematics of the SCM measurements: (*a*) when a negative dc bias voltage is applied on the sample, there are three capacitors, including $C_{\mathrm{O}}$, $C_{\mathrm{d1}}$ and $C_{\mathrm{sub}}$ in series, reflecting dopant distribution of the upper part of the p-type Si; (*b*) when a positive dc bias voltage is applied on the sample, there are two capacitors, including $C_{\mathrm{O}}$ and $C_{\mathrm{d2}}$ in series, reflecting the dopant distribution of the lower part of the p-type Si.

[20]. Therefore, the measured SCM signal, as a result of the variation of the overall capacitance ($\Delta C_T$) at a constant voltage mode of SCM measurement is $\Delta C_T \cong \Delta C_{d1}$ and reflects the dopant distribution in the *upper* part of the p-doped layer. On the other hand, when a positive dc bias voltage is applied on the sample as shown in figure 2(*b*), since there are only two capacitors, including $C_0$ and $C_{\mathrm{d2}}$ in series, $\Delta C_T \cong \Delta C_{d2}$ and the measurement reflects the dopant distribution in the *lower* layer of the p-type Si in the n-well.

The ac bias voltage was set to the maximum value of the SCM system (10 V) to ensure sufficient potential drop [21] on $C_{\mathrm{d1}}$ and $C_{\mathrm{d2}}$ for negative and positive $V_{\mathrm{dc}}$, respectively. We also verified that this high voltage did not cause degradation of the SCM signal. SCM imaging has been observed during AFM scanning along the sample surface. The same probe tip and identical instrument settings were used except that dc bias voltages were set at −5 V and +5 V. Moreover, it was confirmed that those measurements were performed before any significant probe wear occurred by comparing the experimental results on a uniformly step-doped epitaxial Si wafer before and after the measurement of the devices.

## 3. Results and discussion

One major point of SCM detection on our devices is that the obtained SCM contrast of the gaps left after the laser irradiation is different from that obtained in the boron doped links of the laser irradiated area. For the gap without laser melting, for example, when a negative $V_{\mathrm{dc}}$ is applied on the sample (see figure 2(*a*)), carriers (electrons) accumulate at the upper Si layer close to the interface between the dielectric and the Si, and then the large capacitance of the p–n junction, formed by the p-type substrate and n-type well, has only very small variations, yielding a very low SCM contrast. However, when measuring the laser tuned area, a higher SCM contrast appears due to a larger capacitance variation from the additional micro-capacitor of $C_{\mathrm{d1}}$. Those two different contrasts give the chance to measure the dimension of the submicron conductive links. It should be pointed out, as mentioned previously by other researchers [18], that the effect of carrier movement from a region with one dopant type into an adjacent region with a different dopant type will yield a detectable p–n junction movement. Therefore, the measured widths of the submicron conductive links and the gap between the two heavily doped regions would be widened ($|V_{\mathrm{dc}}| > 5$ V) or narrowered ($|V_{\mathrm{dc}}| < 5$ V). In order to avoid those artefacts, the gap width of 600 nm was first measured independently by chemically selective etching in combination with a TEM (transmission electron microscopy) technique [15]. Then, a wide range of $V_{\mathrm{dc}}$ were tested and finally the $V_{\mathrm{dc}}$ values of −5 V and + 5 V were adopted for 2D SCM imaging on our devices because it can reproduce the measured gap of 600 nm.

Due to the importance of topography on SCM measurements, the surface roughness of the microdevices was measured by AFM at the same time as SCM imaging was performed. All the surface morphology of the reoxidized devices, e.g. as shown in figure 3(*a*), is uniform with a root mean square (RMS) roughness of less than ∼0.5 nm, indicating that no deformation was caused by laser irradiation. Therefore, the submicron conductive links cannot be detected by AFM and this very good flatness is ideal for reliable SCM measurements. Figure 3(*b*) shows a SCM image, obtained from a device produced by laser irradiation with a power of 3.10 W and 100 pulses, taken with $V_{\mathrm{dc}}$ of −5 V. An array of three submicron conductive links is revealed. The centre one of the three has lower contrast, probably indicating that the dopant concentration in the local upper regrown region, close to the interface between the dielectric and Si, is higher than the other ones which have probably the same level of dopant concentration. The uncompleted link is probably caused by a misalignment of the laser beam yielding a shorter diffusion time of the dopants [22, 23]. Figure 3(*c*) shows a SCM image taken from a device irradiated by 30 pulses at a power of 3.10 W. There are two completed links formed with a distance of about 700 nm apart. Figures 3(*d*) and (*e*) show an array of 6 submicron conductive links, fabricated by irradiating the sample with 100 pulses of a laser power of 3.75 W. Both images indicate that the central links are slightly wider than those far from the centre. In addition, there is one uncompleted diffused stripe on the left and the right side, respectively, of the conductive array. The reason for this phenomenon is probably that the melting of the Si materials in these areas with sub-maxima of interfering light is not uniform; causing a non-uniform diffusion. For all the micro-devices fabricated by polarized laser irradiation with an intensity of either 3.1 or 3.75 W, the separation ($\Lambda$) of submicron resistive links, including uncompleted links, is about $\Lambda = 360$ nm. This is reasonable if we consider $\Lambda = \lambda/n$ with the values of a laser wavelength ($\lambda$) of 532 nm and an oxide refractive index ($n$) of 1.48 [14].

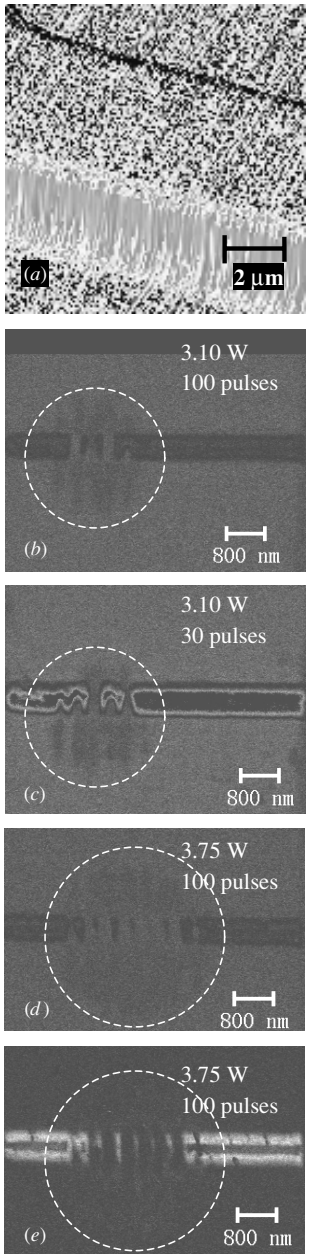


**Figure 3.** (*a*) Three-dimensional AFM image taken from a device irradiated with a laser power of 3.10 W and 100 pulses; (*b*) SCM images taken with dc bias voltages of −5 V from the same device as in (*a*); (*c*) SCM images taken, by applying dc bias voltages of −5 V, from a device irradiated by a laser power of 3.10 W and 30 pulses; (*d*) and (*e*) SCM images obtained from a device irradiated by a laser power of 3.75 W and 100 pulses by applying dc bias voltages of −5 V and +5 V, respectively. The dashed circles represent the melted ranges.

The SCM images, taken under $V_{dc}$ of −5 and +5 V, have similar patterns of dopant distribution for all laser diffused devices. Figure 4 shows the average width of conductive links, extracted from SCM images, in the micro-devices fabricated with a laser power of 3.10 and 3.75 W and for 30, 50 and 100 pulses. Note that all average widths are lower than $\Lambda = 360$ nm corresponding to a uniform melted pool and to the disappearance of the array of submicron links. Error bars were deduced from measurements on many devices (up to

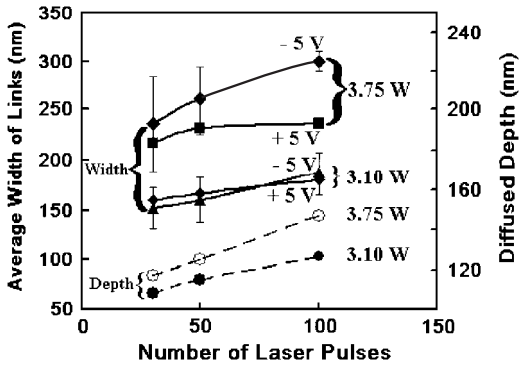


**Figure 4.** Average width of the upper side (dc = −5 V) and lower side (dc = +5 V) of the submicron conductive links formed by laser irradiation with light intensities of 3.10 W and 3.75 W together with the maximum melting depth for both cases.

12 devices for $V_{dc} = -5$ V), each of them having from two to seven submicron links. The variation of the number of conductive links in different devices fabricated under the same conditions of laser intensity and pulse number may be due to the instability of laser interaction with materials which depends on specific delectric/Si interface and the exact characteristics of multilayer materials. The depths of the melted region as determined by performing dopant selective etching in combination with TEM imaging [15] are also given for reference. As the laser power increases, both the depth and the width increase as the melting time and consequently the dopant diffusion time are longer due to the larger energy absorbed by the materials [22]. The increase in the number of laser pulses has a similar effect as from pulse to pulse the accumulated dopant diffusion time increases. Figure 4 also indicates that the upper ($V_{dc} = -5$ V) and lower ($V_{dc} = +5$ V) widths of the links are almost the same for the devices fabricated with a lower laser power (3.10 W) but are clearly different for a higher value (3.75 W) and as the number of laser pulses increases. As will be discussed below, oxygen, which is an n-type dopant in silicon, is probably diffusing from the $SiO_2$ toward the silicon melted poll as the power increases, thus affecting the effective dopant distribution and SCM measurements.

In order to characterize the electrical properties, measurements of $dC/dV$ versus sample bias $V_{dc}$ were carried out in the centre of submicron conductive links and the results are shown in figures 5(*a*) and (*b*) for microndevices fabricated at laser powers of 3.10 W and 3.75 W, respectively. For comparison, the $dC/dV \sim V_{dc}$ curves taken at the heavily doped regions far from the laser irradiated area are also shown. For all those measurements, when the sample is negatively biased, SCM signals in the laser irradiated conductive links are lower than those in the initially heavily doped regions without laser irradiation. Those results indicate that the net carrier concentration in the upper parts of the submicron regrown Si links was higher than that in the initially heavily doped regions. This phenomenon can probably be explained by the fact that the concentration of the net electrical activated dopants that diffused into the upper regions of the submicron conductive links is higher than that in the heavily doped regions without laser melting, probably due to the higher electrical activation

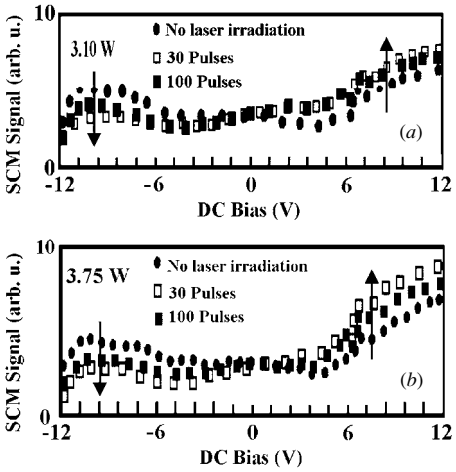


**Figure 5.** $dC/dV$ versus sample bias $V_{dc}$, taken in the centre of submicron resistive links in the microndevices fabricated with a laser power of (*a*) 3.10 W and (*b*) 3.75 W. Results taken in the heavily doped region far from the laser irradiated area (no laser irradiation) are also shown in the figures.

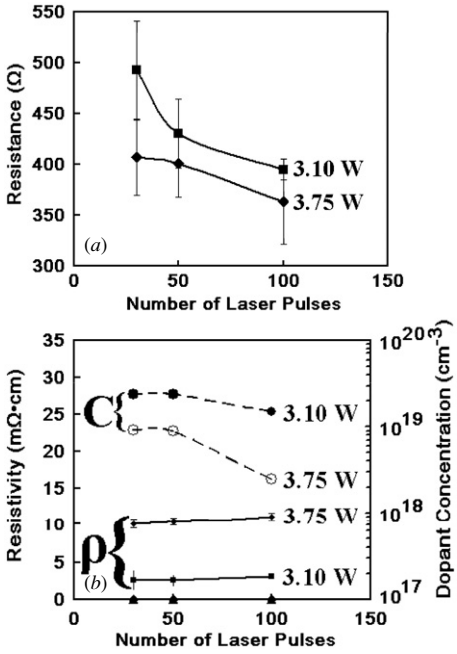


**Figure 6.** Resistance (*a*), and resistivity and dopant dependence (*b*) for laser powers 3.1 and 3.75 W as a function of the number of pulses.

under laser irradiation [24] or boron segregation towards the dielectric multilayers during resolidification. This is in good agreement with the observed higher dopant concentrations, revealed by the lower contrast, in the regrown areas in both the formed conductive links and the laser-irradiated parts of the heavily doped regions, as shown in the SCM images of figures 3(*b*), (*c*) and (*d*), measured at a fixed $V_{dc}$ of $-5$ V. Moreover, it is very interesting to note that the SCM images (not shown here), obtained from microdevices fabricated by laser irradiation under a power of 3.10 W and 30 pulses with a $V_{dc}$ bias of +5 V, had the same contrast difference, between conductive links and non-irradiated heavily doped regions, as that shown in figure 3(*c*). The origin causing these results might be related to the possible fact that the dopant concentration in the regrown conductive links are almost uniform, yielding similar $\Delta C$ with the same ac bias modulation as measured with a $V_{dc}$ of $-5$ V and +5 V. Furthermore, for both cases with laser intensities of 3.75 W and 3.10 W, the SCM signals with a negative $V_{dc}$ reveal that the net carrier concentrations in the conductive links close to the interface between the dielectric and the Si substrate decrease during the irradiation of additional 70 pulses following the irradiation of the first 30 pulses. The reason for this phenomenon might be related to the presence of oxygen in the upper part of the conductive links. Indeed, as either the number of pulses and/or laser power increase, more oxygen atoms diffuse from the $SiO_2$ into the melted Si, thus compensating the effect of the acceptors, because O is know to be an n-type dopant [25].

On the other hand, as shown in figure 5, the shift of SCM signals in the positive $V_{dc}$ range, directed by the arrows from the non-irradiated heavily doped region to conductive links, suggests that the net p-type carrier concentration close to the bottom of the melting pool increases and becomes 'box-like' distribution with the increase of the pulse number from 30 pulses to 100 pulses. In addition, the net carrier concentration in these depth regions of the conductive links with a laser irradiation of 3.75 W is less than that with 3.10 W probably because the melted pool is deeper yielding a lower dopant concentration at the bottom of the link where the SCM probes at $V_{dc} = +5$ V.

Furthermore, as shown in figure 5, the change of the SCM signal decreases as the irradiation time increases when the applied laser power is fixed. This point could be explained by considering that the net electrically activated dopant atoms distribute more uniformly in the melted and regrown regions in devices produced with longer laser irradiation time. This was indeed verified by dopant selective etching (DSE) in combination with TEM analysis in our previous publication [15].

Figure 6(*a*) shows resistance $R$ as obtained by four-point probe measurement as a function of the number of pulses for 3.10 and 3.75 W of laser power. It should be mentioned that the leakage current of the resulting p-link/$N_{Well}$ junction is smaller than 50 pA. The measured resistances are between 363 and 493 Ω and decrease when more pulses and/or higher power are applied, mainly due to the increase in both the molten width and depth, as shown in figure 4. Assuming a uniformly dopant distribution, an average resistivity can be evaluated using $\rho = RA/l$, where $A$ is the total area of $N_L$ half ellipses ($A = N_L \pi wd/8$, where $N_L$ is the number of links and $w$ and $d$ are the width and the depth, respectively, given in figure 4) and $l$ the length taking as the initial gap width of 600 nm. Figure 6(*b*) shows that, on average, $\rho$ are $2.8 \pm 0.3$ and $10.6 \pm 0.6$ mΩ cm for links fabricated at 3.1 and 3.75 W, respectively. In the same figure, the effective dopant concentration is also given by using the experimental relationship between the resistivity and the dopant level [20]. The range of effective dopant concentration between $1.5 \times 10^{18}$ and $2.4 \times 10^{19}$ $cm^{-3}$ is quite reasonable as it must be slightly lower on average, after diffusion, than the doping level

of $5 \times 10^{19}$ acceptors $cm^{-3}$ of the heavily doped regions. The difference between the links made at 3.10 W and 3.75 W and the slight increase in $\rho$ as the number of pulses increases are again probably related to the presence of oxygen contaminants in the links, as proposed by the SCM results above.

## 4. Summary

An array of submicron conductive links was formed in silicon covered by $SiO_2$ by laser induced periodic melting. In this process, under specific polarized laser conditions, the dopants present in the two highly doped regions diffuse into the periodic melt thus forming an array of conductive links joining the two doped regions. As characterized by a four-point probe and SCM measurements, the resistors with submicron conductive links have resistances ranging from 363–493 Ω and their values are related to the width and depth of the links as well as to the dopant and oxygen concentrations. All these characteristics depend on laser intensity and pulse number. The number of submicron conductive links depends mainly on the laser intensity, while the width (151–300 nm) and depth (108–147 nm) of the links depend not only on the laser intensity but also on the pulse number. The quality of the dielectric/Si interface and of the multilayer materials should be well controlled in order to produce arrays with a specific resistance value, number, width and depth of conductive links.

## Acknowledgments

The authors would like to thank Alain Lacourse and Hugo St-Jean from LTRIM Technologies for providing the samples and Dr J-Y Degorce from École Polytechnique de Montréal for very interesting discussions. The financial contribution from the Natural Science and Engineering Research Council (NSERC) of Canada is also acknowledged.

## References

[1] Combescot M and Bok J 1984 *Phys. Rev.* B **29** 6393
[2] Birnbaum M 1965 *J. Appl. Phys.* **36** 3688
[3] Emmony D C, Howson R P and Willis L J 1973 *Appl. Phys. Lett.* **23** 598
[4] Walters C T 1974 *Appl. Phys. Lett.* **25** 696
[5] Isenor N R 1977 *Appl. Phys. Lett.* **31** 148
[6] Theppakuttai S and Chen S 2004 *J. Appl. Phys.* **95** 5049
[7] Keilmann F and Bai Y H 1982 *Appl. Phys.* A **29** 9
[8] Maracas G N, Harris G L, Lee C A and McFarlane R A 1978 *Appl. Phys. Lett.* **33** 453
[9] Sipe J E, Young J F, Preston J S and van Driel H M 1983 *Phys. Rev.* B **27** 1141
[10] Guosheng Z, Fauchet P M and Siegman A E 1982 *Phys. Rev.* B **26** 5366
[11] Young J F, Sipe J E, Preston J S and van Driel H M 1982 *Appl. Phys. Lett.* **41** 261
[12] Fauchet P M and Siegman A E 1982 *Appl. Phys. Lett.* **40** 824
[13] Meunier M, Gagnon Y, Savaria Y, Lacourse A and Cadotte M 2002 *Appl. Surf. Sci.* **186** 52
[14] Liao Y, Degorce J-Y and Meunier M 2005 *Appl. Phys.* A **82** 679
[15] Liao Y, Degorce J-Y, Belisle J and Meunier M 2006 *J. Electrochem. Soc.* **153** G16–G22
[16] Isenbart J, Born A and Wiesendanger R 2001 *Appl. Phys.* A **72** S243–51
[17] Schroder D K 1990 *Semiconductor Material and Device Characterization* (New York: Wiley)
[18] Yamamoto T, Suzuki Y, Miyashita M, Sugimura H and Nakagiri N 1997 *Japan. J. Appl. Phys.* **36** 1922
[19] Nicollian E H and Brews J R 1982 *MOS Physics and Technology* (New York: Wiley) chapter 1
[20] Sze S M 2002 *Semiconductor Devices, Physics and Technology* 2nd edn (New York: Wiley) p 55
[21] Nakagiri N, Yamamoto T, Sugimura H, Suzuki Y, Miyashita M and Watanabe S 1997 *Nanotechnology* **8** A32
[22] Degorce J-Y, Gillet J-N, Magny F and Meunier M 2005 *J. Appl. Phys.* **97** 033520-1
[23] Cohen S S, Wyatt P W, Canter J M and Chapman G H 1989 *IEEE Trans. Electron Devices* **36** 1220–5
[24] Whelan S, La Magna A, Privitera V, Mannino G, Italia M, Bongiorno C, Fortunato G and Mariucci L 2003 *Phys. Rev.* B **67** 075201
[25] Mada Y and Inoue N 1986 *Appl. Phys. Lett.* **48** 1205